RED-TO-BLUE
TTA-UC

Article

Efficient Red−to-Blue Triplet−Triplet Annihilation Upconversion Using the C$_{70}$-Bodipy-Triphenylamine Triad as a Heavy-Atom-Free Triplet Photosensitizer

Yuanming Li,[⊥] Jianhui Zhang,[⊥] San-e Zhu,* Yaxiong Wei, Fan Zhang, Lin Chen, Xiaoguo Zhou,* and Shilin Liu

Read Online

ACCESS | Metrics & More | Article Recommendations | SI Supporting Information

ABSTRACT: Triplet−triplet annihilation upconversion (TTA-UC) with heavy-atom-free organic triplet photosensitizers has attracted extensive attention recently, however, the successful examples with absorption in red and first near-infrared (NIR-I, 650−900 nm) region are still insufficient. Herein, we conducted a new TTA-UC system of perylene using C$_{70}$-bodipy-triphenylamine triad (C$_{70}$-BDP-T) as the heavy-atom-free photosensitizer. Efficient red-to-blue (663 to 450 nm) TTA-UC was achieved in this system with an anti-Stokes shift of 0.88 eV and a quantum yield up to 5.2% (out of a 50% maximum) in deaerated toluene. Notably, this is the highest quantum yield to date in similar TTA-UC systems with heavy-atom-free organic photosensitizers. Using steady-state and transient absorption spectroscopy, together with cyclic voltammo-

gram and quantum chemical calculations, photophysical and photochemical mechanisms were elucidated. Specifically, two triplet triads, C$_{70}$-^{3}BDP*-T and ^{3}C$_{70}$*-BDP-T, were produced efficiently upon photoexcitation, with lifetimes of 2.0 ± 0.1 and 32.2 ± 0.3 μs, respectively. Electron transfer and recombination mechanisms were confirmed to play crucial roles in the formation of these triplets, instead of intersystem crossing. Our results shed light on the superiority of fullerenes in the development of heavy-atom-free photosensitizers.
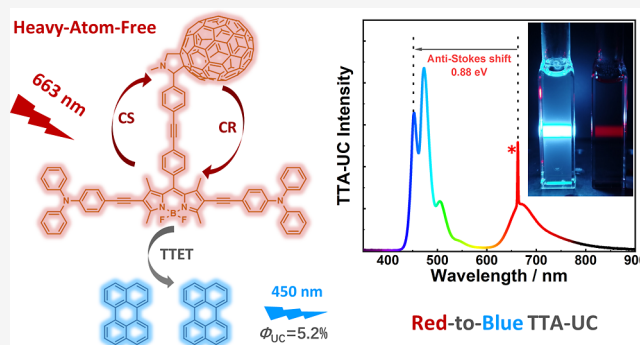
1. INTRODUCTION

Photon upconversion has attracted widespread attention because of its fascinating properties that materials can absorb low-energy light and then emit high-energy photons. In recent years, it has been successfully applied in photovoltaics,[1−3] photocatalysis,[4−6] and bioimaging.[7,8] In comparison to the upconversion method with multiphoton absorptions, triplet−triplet annihilation upconversion (TTA-UC) has specific advantages, such as low light power density, high upconversion quantum yield, and capabilities of adjustable absorption and emission wavelengths.[9,10]

Generally, a TTA-UC system consisted of a photosensitizer and an energy acceptor, in which a consecutive photophysical and photochemical process starts from the low-energy photon absorption of the photosensitizer, and then a long-lived triplet sensitizer is generated via intersystem crossing (ISC). Following the triplet−triplet energy transfer (TTET) from the triplet sensitizer to the acceptor, one singlet excited acceptor is finally produced by the collision-induced TTA process of two triplet acceptors, emitting high-energy photons.[11,12] Thanks to long lifetimes of the triplet photosensitizer and acceptor, the upconversion fluorescence

emission can be greatly extended, so-called "P-type delayed fluorescence".

During the past two decades, many triplet photosensitizers were synthesized for TTA-UC applications. The earliest photosensitizers were mainly transition metal−organic complexes, such as Ru,[13] Pt,[14,15] Pd,[16] Os,[17,18] and Ir,[19] in which the metal atom center significantly enhanced spin−orbit coupling (SOC) of chromophores, leading to a high ISC efficiency. After that, some metal-free organic photosensitizers containing Br and I atoms[20,21] also showed high ISC effect according to the heavy-atom effect. However, the high cost of precious metal and the reduced stability caused by halogen-induced photobleaching[22] limit their applications. Thus, developing heavy-atom-free organic photosensitizers becomes crucial to avoid these disadvantages and meet requirements of
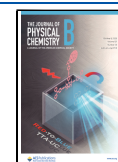
Scheme 1. Molecular Structures of Two Photosensitizers, C$_{70}$-BDP-T and BDP-T, as Well as Two Comparators of C$_{70}$-1 and TPA
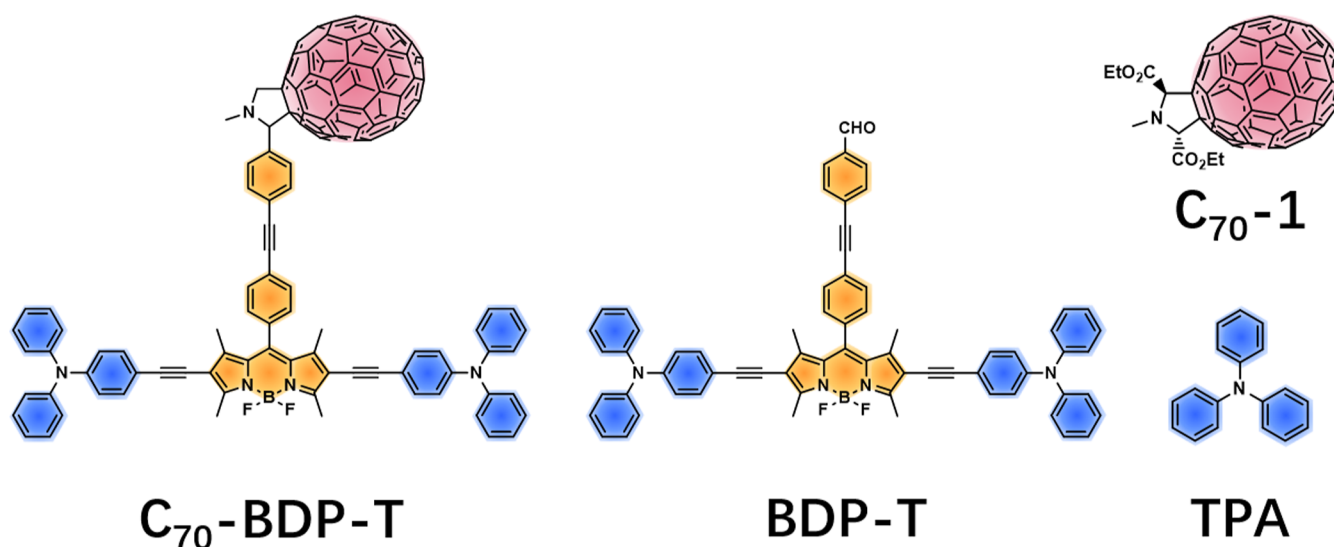
green chemistry.[23] Recently, fullerenes like C$_{60}$ and C$_{70}$ have been commonly used as spin converters in heavy-atom-free photosensitizers, owing to their high ISC efficiencies of nearly unity.[24−32] In addition, the presence of the fullerene moiety also provides another triplet formation mechanism of electron transfer (ELT) and recombination due to the low reduction potentials of fullerene family, besides the enhanced ISC effect.[25,33] Therefore, uncovering the competition between the electron-transfer and the ISC mechanisms in the formation of triplet photosensitizer is valuable for designing the novel fullerene-based photosensitizer in future.

Although the absorption and emission photon energies of the TTA-UC system can be adjusted, most successful TTA examples are limited to the visible to visible (or near ultraviolet) upconversion. We know, for biological applications like bioimaging, near-infrared (NIR) to visible (or ultraviolet) upconversion is highly attractive as the wavelength range of 650−950 nm is well-known as the first confirmed biological tissue transparency window, so-called the NIR-I region.[34−37] A few transition-metal−organic photosensitizers have been reported for high efficient TTA-UC using NIR-I lights.[17,38−40] However, the TTA-UC system containing heavy-atom-free organic photosensitizers with photo-absorption above 650 nm is still limited to date (Table S5).

Pristash et al. reported a 685 to 570 nm TTA-UC system with a quantum yield of 1.5%, in which thiosquaraine and rubrene were used as a photosensitizer and an acceptor, respectively.[9] Recently, Liang et al. constructed a TTA-UC system with dimeric borondifluoride curcuminoid derivative as a photosensitizer and perylene as an acceptor, achieving photon upconversion from 660 to 445 nm with a low quantum yield of 0.4%.[41] When the acceptor was replaced by 9,10-bis[((triisopropyl)silyl)ethynyl]-anthracene, the upconversion fluorescence at 450 nm was observed with the increased quantum yield up to 1.1%.[41] In addition, the upconversion fluorescence was observed at 545 nm with a quantum yield of 0.4% with photoexcitation at 635 nm in the TTA-UC system consisting of helical-bodipy and perylenebisimide,[42] in which the absorption of helical-bodipy (photosensitizer) was extended to the NIR-I window region. Despite these success examples, the reported TTA systems with heavy-atom-free

photosensitizer in the NIR-I window all suffered from relatively low upconversion quantum yields.

Recently, we have synthesized a novel heavy-atom-free triad photosensitizer with the C$_{70}$-bodipy-triphenylamine (C$_{70}$-BDP-T) structure.[43] Scheme 1 shows its molecular structure, along with a comparator, bodipy-triphenylamine (BDP-T) dyad. In contrast to bodipy itself, the triphenylamine (TPA) unit of the triad and dyad increases the conjugation of the bodipy unit, thus extending molecular absorption to the NIR-I region with an onset of 670 nm. As reported previously,[43] the formation efficiency of the corresponding triplet for this triad was remarkably increased due to the contribution of the C$_{70}$ unit. According to the advantages, C$_{70}$-BDP-T might be an excellent heavy-atom-free organic photosensitizer in the NIR-I window for TTA-UC. In this work, we conduct a TTA-UC system of C$_{70}$-BDP-T and perylene (triplet acceptor). The time-resolved transient absorption and fluorescence emission spectroscopy are preformed to validate its red-to-blue upconversion ability and to determine quantum efficiency. Moreover, quantum chemical calculations and cyclic voltam-mogram are carried out to clarify the energy transfer and ELT mechanisms involved in. This highly efficient red-to-blue TTA upconversion is confirmed to be a potentially excellent system with a heavy-atom-free organic photosensitizer for bioimaging or photodynamic therapy applications. These results are of great significance for the development of fullerene-based heavy-atom-free photosensitizers, as well as providing guidance for the exploration of TTA-UC systems in the NIR region.

2. EXPERIMENTS AND COMPUTATIONS

C$_{70}$-BDP-T, BDP-T, and C$_{70}$-1 were synthesized according to the literature.[43] The structures and purities of these compounds were verified using ^{1}H NMR, ^{13}C NMR, and mass spectrometry. The precursors all were analytically pure and were purchased from Sigma-Aldrich Co. and used without any purification.

UV-2550 (Shimadzu) and FP8500 (JASCO) spectropho-tometers were used to measure steady-state UV−vis absorption and fluorescence emission spectra. Nanosecond time-resolved transient absorption spectra were measured with a home-built laser flash photolysis system. The pulsed excitation light (~10
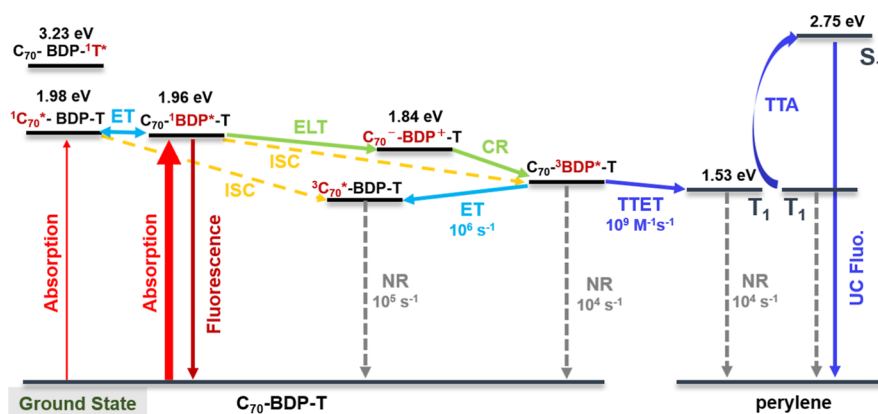
Figure 1. Simplified Jablonski diagram for the TTA upconversion system with C_{70}-**BDP-T** as a photosensitizer and perylene as an annihilator, in which ET is the energy transfer, ELT denotes the electron transfer, CR represents the charge recombination, and NR stands for the non-radiative decay. The relative energies in eV and the approximate rate constants are noted.
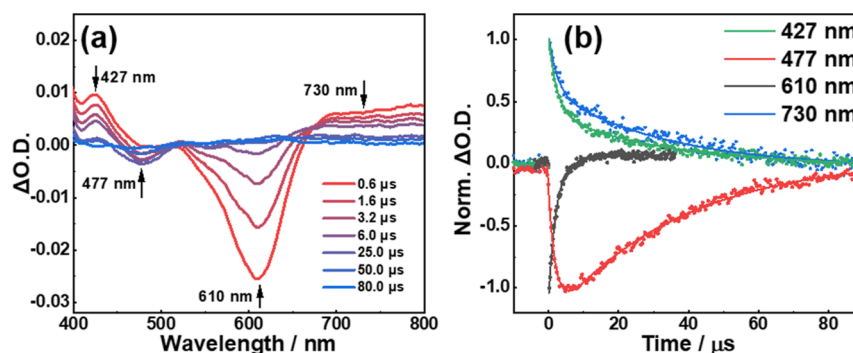

Figure 2. (a) Nanosecond time-resolved transient absorption spectra of C_{70}-**BDP-T** in toluene. (b) Normalized decay curves of the major absorption bands, λ_{ex} = 532 nm.

mJ/pulse) was from the second harmonic 532 nm of a Q-Switched Nd: YAG laser (Dawa-100, Beamtech) with pulse duration of 8 ns and a 10 Hz repetition rate and was intersected by a white light from a 500 W Xenon lamp in a quartz cuvette (10 mm × 10 mm). A monochromator equipped with a photomultiplier (R928, Hamamatsu) was used to record transient absorption spectra within the wavelength range of 400−800 nm, with a spectral resolution of less than 1 nm. A kinetic curve of the intermediate was averaged by multi-shots and recorded with an oscilloscope (TDS3052B, Tektronix). All the solutions were deoxygenated by purging with high purity argon (99.99%) for about 20 min prior to measurements.

TTA upconversion spectra were recorded using a home-made fluorescence emission spectrometer. A semiconductor laser (663 nm) was selected as the excitation light source. The diameter of the laser spot in sample cell region was 3.5 mm. In the upconversion experiments, the solutions mixing photosensitizer and acceptor were kept in a temperature-controlled quartz cuvette (10 mm × 3 mm), deoxygenated by purging with high purity argon for at least 20 min, and the gas flow was maintained during measurements. The upconversion fluorescence of acceptors was collected and detected with a commercial fiber-optic spectrometer (ULS2048-2-USB2, AvaSpec), with the spectral resolution of 1.2 nm.

Cyclic voltammograms were measured at room temperature after purging with argon for 20 min with a scan rate of 50 mV s^{-1}. A three-electrode electrolytic cell was used with tetrabutylammonium hexafluorophosphate (Bu$_4$N[PF$_6$], 0.1

M) as the supporting electrolyte. The working and counter electrodes were the glassy carbon electrode and the platinum electrode, respectively, while the reference electrode was the Ag/AgCl electrode. Dichloromethane was used as the solvent. Ferrocene (Fc) was added as the internal reference.

Geometries of the compounds were optimized using density functional theory (DFT) with the B3LYP function and 6-31G (d) basis set. No imaginary frequencies were verified for all the optimized structures. The spin density surfaces of the C_{70}-**BDP-T** triad, the energy gaps between ground state and lowest triplet state, and the vertical excitation energies were calculated with the time-dependent DFT (TD-DFT) level using the same basis set. The polarizable continuum model[44] was applied to evaluate solvent effects. All these calculations were performed with the Gaussian 16W program package.[45]

3. RESULTS AND DISCUSSION

3.1. Nanosecond Transient Absorption Spectra. As shown in the steady-state absorption spectra of C_{70}-**BDP-T**, **BDP-T**, C_{70}-**1**, and **TPA** in toluene (Figure S1), four major absorptions of the C_{70}-**BDP-T** triad in the UV−visible wavelength range are located at 600, 443, ~400, and 340 nm. By comparing to the spectra of **BDP-T**, C_{70}-**1**, and **TPA**, we can readily achieve their assignments, i.e., the bodipy unit contributes the peaks at 600 and 443 nm, the C_{70} moiety is responsible for the band at ~400 nm and the shoulder peak at 470 nm, and the **TPA** part takes the strongest peak at 340 nm. Given the weak interactions between the functional groups in the C_{70}-**BDP-T** triad, we can derive the singlet excitation

energy of each units from the absorption and fluorescence emission spectra of each monomers, using the strategy proposed by Vandewal et al.[46] As shown in the simplified Jablonski diagram of Figure 1, the corresponding singlet states for the triad is determined to be 1.96 eV for C_{70}-^{1}BDP*-T, 1.98 eV for1C_{70}*-BDP-T, and 3.23 eV for C_{70}-BDP-1T*, respectively. Notably, both the excitation energies of the C_{70} and TPA units are consistent with the data of monomers (2.02 eV for C_{70} and 3.12 eV for TPA),[29,47] while the bodipy one is much lower than the reported value (2.37 eV).[48] Such significant reduction in the excitation energy of bodipy can be explained by the conjugation with the TPA moiety.

According to the absorption spectra, both the bodipy and C_{70} moieties in the triad can be photoexcited at 532 nm, but the former is apparently dominant because of its much larger absorption cross section. Thus, photophysical features of the triad at 532 nm, such as the formation efficiency and lifetime of triplet, can be determined from photoexcitation of the bodipy unit. It is worth noting that the weak fluorescence was observed for the C_{70}-^{1}BDP*-T triad,[43] while the fluorescence quantum yield of BDP-T dyad was high (Figure S2). This phenomenon apparently indicates the efficient singlet energy transfer and the formation of triplets. Considering the energies of the feasible triplets, both C_{70}-^{3}BDP*-T and $^3C_{70}$*-BDP-T might be formed from C_{70}-^{1}BDP*-T, as shown in Figure 1.

To verify the formation of the two triplets, nanosecond time-resolved transient absorption spectra of C_{70}-BDP-T in deaerated toluene with photoexcitation at 532 nm were measured and are plotted in Figure 2a. In contrast to the previously reported spectra,[43] it is surprising that more details emerge as we have optimized experimental conditions. Besides the two positive bands at 427 and >700 nm and a negative peak at 477 nm which are identical to the previous results,[43] a negative peak at 610 nm with faster attenuation is clearly observed. Considering the absorptions of the bodipy and C_{70} units at 600 and 470 nm, respectively, the negative peaks at 610 and 477 nm are naturally attributed to ground-state bleaching (GSB) bands of the bodipy and C_{70} moieties. On the other hand, the two positive peaks at 427 and 730 nm are attributed to absorptions of triplets.

As the decay of the GSB band is closely related to the formation of triplet states, the evolution dynamics of the GSB intensities at 610 and 477 nm can indicate the population changes of the triplet bodipy and C_{70} units in the triad, respectively. Figure 2b shows the decay kinetics at 610 and 477 nm in current conditions. To our surprise, two GSB curves display completely distinct kinetic behaviors, strongly suggesting that there are two different triplet states formed upon photo-excitation. The formation and decay of the GSB band at 477 nm (the red trace in Figure 2b) are remarkably later than the evolution of the GSB at 610 nm (in black), and hence, the triplet C_{70} unit looks like being formed just with the consumption of the triplet bodipy moiety (Figure 2b). As shown in Figure S3, the GSB peak of the bodipy moiety at 610 nm can be well-fitted by a single-exponential decay, leading to a moderate lifetime of 2.0 ± 0.1 μs for the triplet bodipy moiety (noted as C_{70}-^{3}BDP*-T in following discussions). In comparison, a global fitting of the decay dynamics at 477 nm for the C_{70} GSB band suggests a formation rate of 5.0 ± 0.3 × 10^5 s^{-1} (corresponding to the lifetime of 2.0 ± 0.1 μs) and a decay rate of 3.1 ± 0.3 × 10^4 s^{-1} (32.2 ± 0.3 μs lifetime), respectively. In other words, the formation and decay rates of $^3C_{70}$*-BDP-T in current conditions are determined. Notably,

an excellent consistence exists between the decay rate of C_{70}-^{3}BDP*-T and the $^3C_{70}$*-BDP-T formation rate, validating that C_{70}-^{3}BDP*-T is preferentially produced upon the formation of C_{70}-^{1}BDP*-T in photoexcitation, then $^3C_{70}$*-BDP-T is subsequently formed via the intramolecular triplet energy transfer from the bodipy unit to the C_{70} moiety.

As shown in Figure 2b, kinetics of the two positive peaks at 427 and 730 nm both exhibit double-exponential decay features. Thus, using least-square fitting with a double-exponential decay function (in Figure S3), the corresponding lifetimes of the fast and slow components are determined to be 2.3 ± 0.1 and 32.0 ± 0.3 μs for the 427 nm band and 2.4 ± 0.1 and 33.4 ± 0.4 μs for that at 730 nm. The almost same characteristic lifetimes for these two bands are evidently attributed to their identical spectral contributors. Moreover, it is worth noting that the lifetimes of the fast components for these two bands (2.3–2.4 μs) perfectly agree with the C_{70}-^{3}BDP*-T lifetime (2.0 μs), and those of the slow components (32.0–33.4 μs) are greatly consistent with the $^3C_{70}$*-BDP-T lifetime (32.2 μs). Therefore, the two positive peaks are assuredly ascribed to the co-absorption of the C_{70}-^{3}BDP*-T and $^3C_{70}$*-BDP-T triplets. Although the same contributors are assigned for the two absorption bands at 427 and 730 nm, their kinetic behaviors are not identical in Figure 2b due to prominent disparities in the fast and slow component weights. From the double-exponential fitting, the weight ratios of the fast component to the slow one are determined to be 1.53 at 427 nm and 0.76 at 730 nm, respectively. Apparently, the weight inequalities arise from different absorption cross sections of C_{70}-^{3}BDP*-T and $^3C_{70}$*-BDP-T at 427 and 730 nm.

To further substantiate the assignments, the transient absorption spectrum of BDP-T dyad was measured with photoexcitation at 532 nm (Figure S4) for comparison. Because only triplet bodipy moiety can be produced in this case, the observed GSB peak at 610 nm and two positive absorption bands at 427 and >700 nm exclusively come from the triplet bodipy unit. Based on the fact that these absorptions were both observed in Figures 2a and S4, we have high confidence in the aforementioned spectral assignments.

3.1.1. Formation Mechanism of Triplet Triad. As indicated in Figure 1, the triplet triad, C_{70}-^{3}BDP*-T, can be formed along two possible thermodynamic pathways. One is the direct ISC process from C_{70}-^{1}BDP*-T to C_{70}-^{3}BDP*-T, while the other occurs via ELT and charge recombination (CR) processes, i.e., C_{70}-^{1}BDP*-T → C_{70}^--BDP$^+$-T → C_{70}-^{3}BDP*-T. We know that the SOC of the bodipy unit might be enhanced when attached to a conjugated chromophore.[49−51] However, as shown in Figure S2, the strong fluorescence emission at 664 nm was still observed from the bodipy unit of the BDP-T dyad upon photoexcitation, indicative of an insignificant influence on the ISC efficiency induced by the TPA moiety. Moreover, in our previous study of C_{70}-Bodipy dyad with initially photoexcited bodipy moiety,[48] the unique triplet, $^3C_{70}$*-Bodipy, was observed in transient absorption spectra, and no experimental evidence was found for the existence of C_{70}-^{3}Bodipy*. Thus, the SOC effect of bodipy enhanced by the C_{70} moiety should be insignificant too. Accordingly, the triad triplet of C_{70}-^{3}BDP*-T dominantly originates from the ELT-CR mechanism. In other words, a charge-separated state (CSS), C_{70}^--BDP$^+$-T, is preferentially produced owing to the low reduction potential of the C_{70} unit, following the intramolecular CR process.
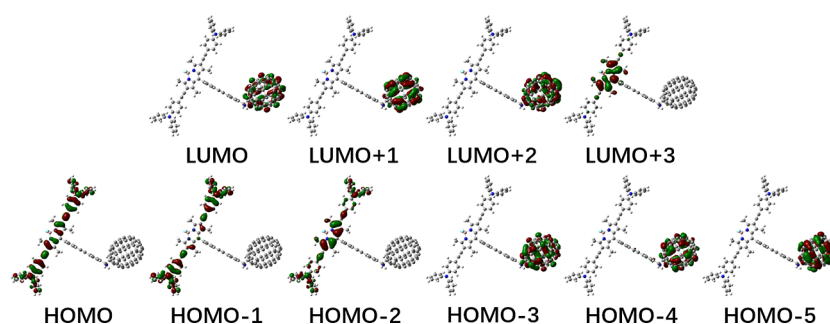
Figure 3. Frontier molecular orbitals of C_{70}-BDP-T.

In the ELT process, negative Gibbs free energies of charge-separation (ΔG_{CS}) and charge-recombination (ΔG_{CR}) processes are the most important driving force for the ELT-CR mechanism. Herein, we calculated the ΔG_{CS} and ΔG_{CR} values and the relative energy of CSS (E_{CSS}) for the C_{70}^{-}-BDP^{+}-T using the Weller eqs 1−3

$$\Delta G_{CS} = E_{ox}(BDP^{+}/BDP) - E_{red}(C_{70}/C_{70}^{-}) - E_{0-0} + \Delta G_S \quad (1)$$

$$\Delta G_{CR} = -[E_{ox}(BDP^{+}/BDP) - E_{red}(C_{70}/C_{70}^{-})] - \Delta G_S \quad (2)$$

$$E_{CSS} = E_{ox}(BDP^{+}/BDP) - E_{red}(C_{70}/C_{70}^{-}) + \Delta G_S \quad (3)$$

where $E_{ox}(BDP^{+}/BDP)$ and $E_{red}(C_{70}/C_{70}^{-})$ are the oxidation and reduction potentials of bodipy (electron donor) and C_{70} (electron acceptor) units, respectively, and ΔG_S denotes the static Coulombic energy as calculated with eq 4

$$\Delta G_s = -\frac{e^2}{4\pi\varepsilon_0\varepsilon_s R_{CC}} - \frac{e^2}{8\pi\varepsilon_0}\left(\frac{1}{R_D} + \frac{1}{R_A}\right)\left(\frac{1}{\varepsilon_{REF}} - \frac{1}{\varepsilon_s}\right) \quad (4)$$

where e represents electronic charge and ε_0, ε_S, and ε_{REF} refer to vacuum permittivity and dielectric constants of solvents used for photochemical and electrochemical measurements, respectively. The solvents used in the experiments were dichloromethane ($\varepsilon_S = 2.24$) and toluene ($\varepsilon_{REF} = 9.1$). R_{CC} is the center-to-center separation distance between donor and acceptor, which is determined to be 19.5 Å in the DFT-optimized geometry. R_D and R_A are the radius of the electron donor and acceptor, which are 15.4 and 5.3 Å, respectively, as the maximum extension radius of molecular electron cloud in space. E_{0-0} stands for the adiabatic excitation energy to form C_{70}-$^1BDP^*$-T, which is experimentally determined to be 1.96 eV as the crossing point of the absorption and fluorescence spectra, as suggested by Vandewal et al.[46]

Besides, the oxidation potential and reduction potentials of C_{70}-BDP-T were determined from cyclic voltammogram. As illustrated in Figure S7, C_{70}-BDP-T exhibits three reversible oxidation waves at +0.82, +0.92, and +1.23 V, as well as two reversible reduction waves at −0.74 and −1.05 V, respectively. In the previous study of C_{70} monomer,[48] one-electron reversible reduction waves were observed at the approximate potentials without any oxidation peaks. Thus, the three oxidation waves of the triad are attributed to the bodipy moiety, which were likewise observed in other bodipy derivatives.[52] Based on these assignments (in Table S1), the ΔG_S, ΔG_{CS}, ΔG_{CR}, and E_{CSS} values of C_{70}-BDP-T in deaerated toluene were determined to be +0.28, −0.12, −1.84, and +1.84

eV, respectively. Apparently, the negative ΔG_{CS} provides significant driving force for the intramolecular charge separation of the excited triad, that is, the photo-induced ELT between the bodipy unit and the C_{70} moiety is thermodynamically allowed. Apparently, this efficient ELT-CR mechanism ensures the higher formation efficiency (78%) of the triplet C_{70}-BDP-T than that of BDP-T (<1%).

To further reveal the nature of the excited states of the C_{70}-BDP-T triad, we calculated their optimized geometries, relative energies, and electronic transition properties. Frontier molecular orbitals of the triad were analyzed using the corresponding optimized geometries and are shown in Figure 3. HOMO and HOMO-2 are spread throughout the skeleton of bodipy and TPA units, and HOMO-1 is mainly located on TPA, while HOMO-3, HOMO-4, and HOMO-5 are contributed by the C_{70} moiety. LUMO, LUMO + 1, and LUMO + 2 are attributed to C_{70}, while LUMO + 3 is exclusively distributed on the bodipy unit.

As illustrated in Table S3 and Figure S8, the formation of the lowest singlet state (S_1) is calculated to be negligible due to too weak HOMO → LUMO transition, while the absorption of the bodipy unit is dominant with the transition of HOMO to LUMO + 3. Notably, the HOMO → LUMO + 3 transition shows a partial charge-transfer property, as indicated by the HOMO and LUMO + 3 in Figure 3. The excitation of the C_{70} moiety is associated with the transition from HOMO − 4 (or HOMO − 5) to LUMO + 1, and the corresponding oscillator strengths are much lower than the bodipy absorption (Table S3), which is in accordance with the experimental conclusion that the dominantly photoexcited functional group at 532 nm for the triad is located at the bodipy moiety. Moreover, the T_1 and T_2 states were attributed to the transitions of HOMO → LUMO + 3 and HOMO − 3 → LUMO, respectively, thus namely C_{70}-$^3BDP^*$-T and $^3C_{70}^*$-BDP-T. At each own optimized geometry, adiabatic excitation energies were calculated to be 1.30 eV for T_1 and 1.35 eV for T_2. Thus, the intramolecular triplet energy transfer between C_{70}-$^3BDP^*$-T and $^3C_{70}^*$-BDP-T observed in the experiment is thermodynamically feasible according to their approximate energies, especially taking in account thermal activation at room temperature.

In addition, there is another possible pathway to form these triplets, i.e., C_{70}-$^1BDP^*$-T ↔ $^1C_{70}^*$-BDP-T → $^3C_{70}^*$-BDP-T, according to the Jablonski diagram (Figure 1). However, in experiments we observed the formation of C_{70}-$^3BDP^*$-T prior to $^3C_{70}^*$-BDP-T (Figure 2b), implying that the path of C_{70}-$^1BDP^*$-T ↔ $^1C_{70}^*$-BDP-T → $^3C_{70}^*$-BDP-T plays an inconsequential role in comparison to the ELT-CR process. Based on this conclusion, we can boldly speculate that the
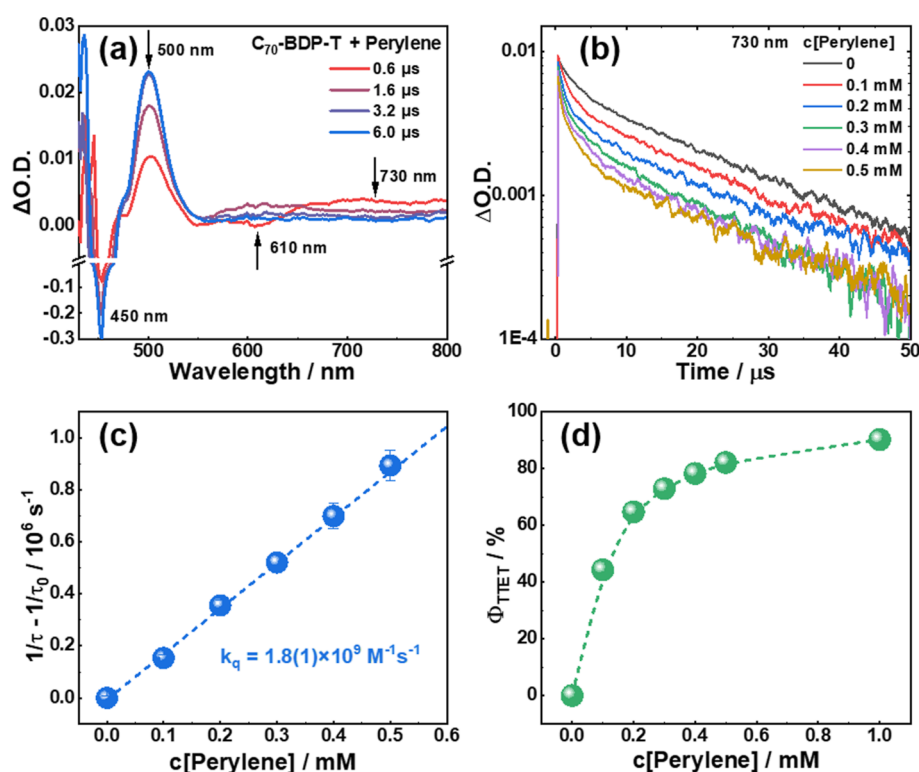
Figure 4. (a) Nanosecond time-resolved transient absorption spectra of C_{70}-BDP-T with perylene (1×10^{-3} M) as an acceptor. (b) Decay curves at 730 nm of C_{70}-BDP-T with different concentrations of perylene in logarithmic coordinate. (c) Bimolecular quenching rate generated from the triplet-state lifetime quenching curves of C_{70}-BDP-T with different concentrations of perylene. (d) TTET efficiency between C_{70}-BDP-T and perylene as a function of the perylene concentration.

intramolecular ELT rate from the bodipy to C_{70} units in the triad is much faster than the ISC rate of the C_{70} moiety ($\sim 10^8$ s^{-1}).[29] Apparently, more detailed dynamic information require a femtosecond time-resolved transient absorption experiment, which is undergoing but beyond the scope of this paper, since our attention are mainly paid on the subsequent TTA upconversion efficiency.

3.1.2. TTET between C_{70}-BDP-T and Perylene. With the addition of perylene as an energy acceptor, the GSB peak at 610 nm quickly disappears in the transient absorption spectra, while a new negative peak at 450 nm and a positive absorption at 500 nm are simultaneously enhanced within a few microseconds, as shown in Figure 4a. According to the well-assigned reference,[53,54] these two forming transient bands are attributed to the GSB of perylene and the absorption band of triplet perylene, respectively, confirming the efficient TTET from the triplet triad (C_{70}-^{3}BDP*-T or $^3C_{70}$*-BDP-T) to perylene. By monitoring the decay dynamics of the absorption band of the triplet photosensitizer at 730 nm, we derived the corresponding triplet lifetimes from the curve-fitting. Notably, these curves in the presence of perylene at various concentrations exhibit double-exponential decay variations (Figure 4b), and the corresponding lifetimes of two components are listed in Table S2.

To our surprise, only decay rate of the fast component (assigned to C_{70}-^{3}BDP*-T as mentioned above) was varied with the perylene concentration, while the slow one corresponding to $^3C_{70}$*-BDP-T remains almost constant. This apparently unusual phenomenon indicates that the TTET only occurs between C_{70}-^{3}BDP*-T and perylene in current conditions. This is opposite to the general rule that a

longer triplet lifetime is conductive to the bimolecular energy transfer. Actually, the triplet energy of perylene was reported as 1.53 eV,[55] while the T_1 of C_{70} monomer was determined to be 1.55 eV from the phosphorescence spectrum.[56] Considering that the triplet energy of the C_{70} unit in the triad might be further lowered due to the conjugative effect, the TTET of $^3C_{70}$*-BDP-T + Pr (perylene) $\rightarrow$ C_{70}-BDP-T + ^{3}Pr* should be slightly endothermic and difficult to occur. In contrast, another TTET process of C_{70}-^{3}BDP*-T + Pr $\rightarrow$ C_{70}-BDP-T + ^{3}Pr* is apparently exothermic. Therefore, the energetics leads to the specific TTET phenomenon between the triplet triad and perylene. In other words, the current experimental results give an unquestionable sequence of three triplet-state energy levels, C_{70}-^{3}BDP*-T > ^{3}Pr* > $^3C_{70}$*-BDP-T, although the DFT calculations yield the three triplet energies close to each other, and the differences are within the calculation uncertainty.

Using the obtained triplet lifetimes in Table S2, the bimolecular quenching rate constant (k_q) and the TTET quantum efficiency (Φ_{TTET}) were calculated according to eqs 5 and 6, respectively

$$\frac{1}{\tau} - \frac{1}{\tau_0} = k_q \cdot [\text{perylene}] \tag{5}$$

$$\Phi_{TTET} = \frac{k_q \cdot [\text{perylene}]}{k_q \cdot [\text{perylene}] + k_T} = \frac{1/\tau - 1/\tau_0}{1/\tau} \tag{6}$$

where τ_0 and τ represent the triplet lifetime of C_{70}-^{3}BDP*-T (the fast component in Table S2) in the absence and presence of perylene, respectively, and k_T is the self-quenching rate of the photosensitizer triplet as $k_T = 1/\tau_0$. Figure 4c plots the
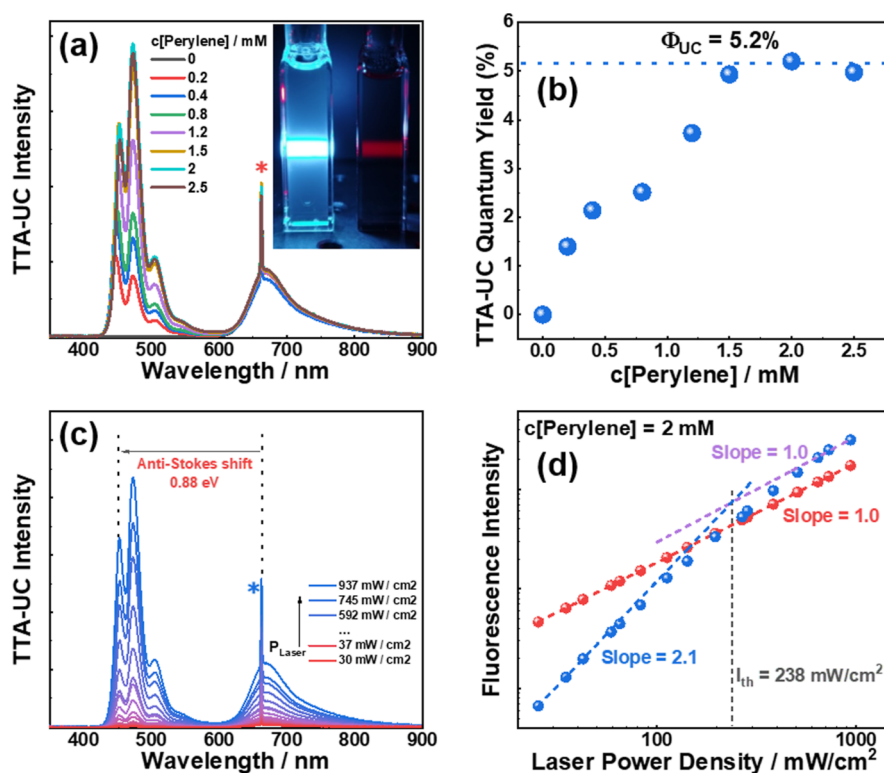
Figure 5. (a) Fluorescence emission spectra of C_{70}-BDP-T and perylene in various concentrations with photo-excitation at 663 nm, where the inset shows the photograph taken with a 500 nm short-pass filter in the presence (left) or absence (right) of perylene (1.5×10^{-3} M). (b) Relationship of the TTA upconversion quantum yield with the perylene concentration. (c) Dependence of the upconversion fluorescence intensity on the excitation power density. (d) Double logarithmic plot of the integrated TTA upconversion fluorescence intensity (blue dots) with the excitation power density, as well as the dependence of the remnant fluorescence intensity (red dots) of C_{70}-BDP-T at 700 nm.

linear relationship between $1/\tau - 1/\tau_0$ and the perylene concentration, resulting in the k_q value between C_{70}-^{3}BDP*-T and perylene of $1.8 \pm 0.1 \times 10^9$ M^{-1} s^{-1}, which is much higher than those in similar systems, e.g., 0.38×10^9 M^{-1} s^{-1} for C_{70}-**Bodipy**[48] and 0.58×10^9 M^{-1} s^{-1} for C_{60}-**Bodipy**.[24] Considering that the triplets in C_{70}-**Bodipy** and C_{60}-**Bodipy** dyads are located on fullerene moiety, this significant improvement of k_q provides additional evidence for the involvement of C_{70}-^{3}BDP*-T in the TTET process. Moreover, we know that the TTET efficiency (Φ_{TTET}) can be influenced by the acceptor concentration, as shown in Figure 4d. Apparently, a satisfactory Φ_{TTET} value of higher than 90% was achieved when the perylene concentration exceeded 1×10^{-3} M.

3.1.3. Triplet−Triplet Annihilation Upconversion of Perylene.

Using C_{70}-BDP-T as a photosensitizer and perylene as an acceptor, we carried out upconversion fluorescence measurements of this new TTA-UC system. With photo-excitation at 663 nm, strong blue fluorescence was observed in deaerated toluene as we expected. Figure 5a shows the TTA-UC fluorescence emission spectra with various perylene concentrations. The upconversion fluorescence covers the wavelength range of 440−540 nm, which is identical with the fluorescence spectrum of perylene itself, supporting the occurrence of photon upconversion. In addition, the remnant fluorescence of C_{70}-BDP-T remains even in the presence of perylene (in Figure 5a), pointing to the fact that the emission of the photosensitizer originates from primary fluorescence that is independent of the triplet energy-transfer procedures. As reported in the previous experiment,[43] the fluorescence

quantum yield of C_{70}-BDP-T in toluene was 4% with photoexcitation at 605 nm, which is comparable to the TTA-UC.

We know that high acceptor concentration facilitates the TTET process and usually improves the TTA-UC efficiency. However, the high concentration may cause pronounced self-absorption or formation of excimers, thereby reducing fluorescence intensity. Therefore, an optimized concentration is necessary for maximizing the upconversion efficiency. As depicted in Figure 5a, the upconversion fluorescence intensity gradually increases with the perylene concentration and saturates when the concentration exceeds 1.5×10^{-3} M. Notably, the relative intensity of the highest energy peak at 450 nm in the fluorescence spectra is reduced with the increase of the perylene concentration, affirming the self-absorption and "secondary inner filter effect". Actually, this phenomenon is common in the visible-to-ultraviolet upconversion systems.[57,58]

Using methylene blue as the standard (fluorescence quantum yield Φ_{std} = 4% in ethanol),[59] the TTA-UC quantum yield, Φ_{UC}, was calculated with eq 7, by integrating the emission band area (400−600 nm) in the fluorescence spectra.

$$\Phi_{UC} = \Phi_{std} \cdot \left(\frac{A_{std}}{I_{std}} \right) \left(\frac{I_{sam}}{A_{sam}} \right) \left(\frac{\eta_{sam}}{\eta_{std}} \right)^2 \tag{7}$$

where A, I, and η are the absorbance intensity, the integrated emission intensity, and the refractive index of the solvents, and "std" and "sam" represent standard and samples, respectively. Notably, as suggested by Castellano et al., the theoretical maximum of Φ_{UC} is defined as 50%.[60] Figure 5b shows the

dependence of Φ_{UC} on the perylene concentration. Apparently, a maximal Φ_{UC} value of 5.2% is obtained at the perylene concentration of >1.5 × 10⁻³ M. It is worth noting that this is the highest TTA-UC quantum yield using heavy-atom-free organic photosensitizer in the NIR-I window to date.

Moreover, as another important parameter of the TTA-UC system, the anti-Stokes shift is determined to be 0.88 eV as the energy difference between the excitation photon and the upconversion fluorescence photon (using the highest energy peak at 450 nm). In addition, the TTA-UC fluorescence intensity correlates quadratically with laser power density at low excitation intensity and linearly at high intensity, with the threshold excitation intensity I_{th} defined by the intersection point.[61−63] As shown in Figure 5c, both the upconversion fluorescence (440−540 nm) of perylene and the remnant fluorescence (620−820 nm) intensity of C_{70}-BDP-T are gradually enhanced with laser power. However, these two fluorescence components exhibit difference dependence on the laser power density. As shown in Figure 5d, there is a slope change from 2 to 1 in the double logarithmic plot for the upconversion fluorescence component, leading to the I_{th} value for TTA-UC of 238 mW/cm². In contrast, the remnant fluorescence of C_{70}-BDP-T shows a linear relationship with laser power density.

Once the triplet state of perylene is generated, its attenuation mainly passes through phosphorescence and non-radiative decay as the first-order process or the TTA process as the second-order reaction. Hence, the rate equation for triplet perylene in the differential form can be expressed as

$$\frac{d[^3\text{perylene*}]}{dt} = -k_T[^3\text{perylene*}] - k_{TTA}[^3\text{perylene*}]^2 \tag{8}$$

where $[^3\text{perylene*}]$ represents the concentration of triplet perylene and k_T and k_{TTA} stand for the first-order and second-order rate constants, respectively. The analytical solution to eq 8 is given by[63,64]

$$[^3\text{perylene*}] = [^3\text{perylene*}]_0 \frac{1-\beta}{e^{k_T t} - \beta} \tag{9}$$

where β indicates the initial proportion of triplet perylene decaying through the second-order channel (TTA), denoted as $\beta = \frac{k_{TTA}[^3\text{perylene*}]_0}{k_T + k_{TTA}[^3\text{perylene*}]_0}$. We know that the upconversion fluorescence intensity (I_{UC}) is proportional to the concentration of singlet excited perylene, $[^1\text{perylene*}]$, which can be simply calculated by $[^1\text{perylene*}] = \frac{k_{TTA}}{k_{FL}}[^3\text{perylene*}]^2$ (k_{FL} is the fluorescence radiation rate of perylene in the S_1 state). Thus, the time-dependent I_{UC} can be expressed as eq 10

$$I_{UC} \propto [^1\text{perylene*}] \propto [^3\text{perylene*}]^2 = [^3\text{perylene*}]_0^2$$
$$\left(\frac{1-\beta}{e^{k_T t} - \beta}\right)^2 \tag{10}$$

By fitting the kinetic curve of normalized upconverted fluorescence at 450 nm (Figure S7), we obtained k_T of 1.7 × 10⁴ s⁻¹ for the triplet perylene and β value of 0.58. In comparison with the C_{60}-Bodipy/perylene in toluene (k_T = 2.4 × 10³ s⁻¹, β = 0.931),[53] the current β value is significantly reduced, accompanying with the enhanced k_T. Given that radiative decay rate of ^{3}perylene* remains in the C_{70}-BDP-T/

perylene and C_{60}-Bodipy/perylene systems, the remarkably increased k_T is readily attributed to the promoted non-radiative decay. However, collision quenching and ISC from T_1 to S_0 are identical for the triplet perylene in the two TTA-UC systems; thus, the k_T variation should be caused by the thermodynamically allowed energy transfer from ^{3}perylene* to $^3C_{70}$*-BDP-T. In this respect, perylene is not the best acceptor for the maximal upconversion quantum yield, and a new acceptor with the slightly lower triplet energy is expected for achieving the higher TTA efficiency at the expense of a little loss of anti-Stokes shift. The corresponding efforts are ongoing.

The quantum yield of the TTA process can be given by $\Phi_{TTA} = 1/2 \cdot f \cdot f_0$, where f_0 represents the proportion of ^{3}perylene* which decay via the bimolecular reaction to the overall channels, which can be calculated by eq 11.

$$f_0 = [^3\text{perylene*}]_0^{-1} \int_0^\infty k_{TT}[^3\text{perylene*}]^2 dt$$
$$= 1 - \frac{\beta - 1}{\beta}\ln(1 - \beta) \tag{11}$$

For the current C_{70}-BDP-T/perylene system, f_0 equals 0.372. Moreover, f denotes spin-statistical factor, which is an important parameter in the TTA process defined as the probability to obtain a singlet excited state (S_1) by the annihilation of two triplet states (T_1). According to the spin-statistical law,[57,65,66] the f value should equal 1/9. However, considering that the formation of quintet excited state usually is energetically forbidden, the quintet coupling pair will split back into two T_1 state to participate in further annihilations. Besides, the decomposition of the triplet-pair encounter always produces a high-energy triplet state like T_2, which can quickly decay to the T_1 state by internal conversion. In this case, the S_1 state and T_1 state will be formed with a statistical ratio of 1:3 during an annihilation process, leading to a higher spin-statistical factor of f = 2/5. On the contrary, when the T_2 energy is higher than double of T_1 state, this channel is energetically forbidden, and the unique fate for the triplet pair is to dissociate reversely into two free T_1 states. In the latter case, each coupling pair can produce one S_1 state, giving an upper limit of f = 1.[67,68]

According to the Jablonski diagram, the overall upconversion quantum yield Φ_{UC} can be expressed as $\Phi_{UC} = \Phi_{ST} \cdot \Phi_{TTET} \cdot \Phi_{TTA} \cdot \Phi_{FL}$. As mentioned above, Φ_{UC} is 0.031 at the perylene concentration of 1 mM. Φ_{ST} represents the formation efficiency of triplet state via ISC and/or ELT-CR mechanisms, which can be estimated as 0.960 for C_{70}-BDP-T. The TTET efficiency, Φ_{TTET}, is 0.901 at 1 mM perylene (in Figure 4d). Φ_{FL} stands for the fluorescence efficiency of perylene, which was measured to be 0.501 in toluene.[48] Using these values, Φ_{TTA} can be calculated to be 0.072, and then, the spin-statistical factor f in this TTA-UC system is determined to be 0.387. As this value is very close to 2/5, the pathway of $T_1 + T_1 \Leftrightarrow {}^3(T_1T_1) \rightarrow T_2 + S_0 \xrightarrow{IC} T_1 + S_0$ plays a pivotal role for the TTA of perylene in toluene.

4. CONCLUSIONS

In this work, we constructed a new TTA-UC system using a recently synthesized heavy-atom-free photosensitizer, C_{70}-BDP-T triad. As the absorption of the bodipy moiety in this triad extends to the NIR-I region due to the conjugation effect of the TPA unit, we successfully achieved highly efficient red-

to-blue (663 to 450 nm) TTA-UC with perylene as the triplet acceptor, with an anti-Stokes shift of 0.88 eV and a quantum yield up to 5.2% (out of a 50% maximum) in deaerated toluene. According to these record-setting values to date, the current system shows an excellent example for highly efficient TTA-UC with heavy-atom-free organic photosensitizers in the wavelength region close to the NIR-I window. These results not only fully demonstrate the superiority of fullerenes in the development of heavy-atom-free photosensitizers but also can serve as a cornerstone for the future design of fullerene derivatives photosensitizers for TTA-UC in the NIR region.

■ ASSOCIATED CONTENT

Ⓢ Supporting Information

The Supporting Information is available free of charge at https://pubs.acs.org/doi/10.1021/acs.jpcb.3c04660.

Steady-state absorption and fluorescence emission spectra and dynamics, additional nanosecond time-resolved transient absorption spectra and kinetic curves, cyclic voltammogram, TTA fluorescence kinetic curve, spectral fitting, transition information, optimized geometry, and summary of the reported TTA-UC systems (PDF)

■ AUTHOR INFORMATION

Corresponding Authors

　San-e Zhu − *School of Energy, Materials and Chemical Engineering, Hefei University, Hefei 230601, China*; Email: zhuse@hfuu.edu.cn

　Xiaoguo Zhou − *Department of Chemical Physics, University of Science and Technology of China, Hefei, Anhui 230026, China*; ⬡ orcid.org/0000-0002-0264-0146; Email: xzhou@ustc.edu.cn

Authors

　Yuanming Li − *Department of Chemical Physics, University of Science and Technology of China, Hefei, Anhui 230026, China*

　Jianhui Zhang − *School of Energy, Materials and Chemical Engineering, Hefei University, Hefei 230601, China*

　Yaxiong Wei − *School of Physics and Electronic Information, Anhui Normal University, Wuhu, Anhui 241000, China*

　Fan Zhang − *Department of Chemical Physics, University of Science and Technology of China, Hefei, Anhui 230026, China*

　Lin Chen − *School of Physics and Materials Engineering, Hefei Normal University, Hefei 230601, China*

　Shilin Liu − *Department of Chemical Physics, University of Science and Technology of China, Hefei, Anhui 230026, China*

Complete contact information is available at:
https://pubs.acs.org/10.1021/acs.jpcb.3c04660

Author Contributions

[⊥]Y.L. and J.Z. contributed equally to this work.

Notes

The authors declare no competing financial interest.

■ ACKNOWLEDGMENTS

■ REFERENCES

(1) Hill, S. P.; Hanson, K. Harnessing Molecular Photon Upconversion in a Solar Cell at Sub-Solar Irradiance: Role of the Redox Mediator. *J. Am. Chem. Soc.* **2017**, *139*, 10988−10991.

(2) Frazer, L.; Gallaher, J. K.; Schmidt, T. W. Optimizing the Efficiency of Solar Photon Upconversion. *ACS Energy Lett.* **2017**, *2*, 1346−1354.

(3) Albinsson, B.; Olesund, A. Untapping solar energy resources. *Nat. Photonics* **2020**, *14*, 528−530.

(4) Ravetz, B. D.; Pun, A. B.; Churchill, E. M.; Congreve, D. N.; Rovis, T.; Campos, L. M. Photoredox catalysis using infrared light via triplet fusion upconversion. *Nature* **2019**, *565*, 343−346.

(5) Monguzzi, A.; Oertel, A.; Braga, D.; Riedinger, A.; Kim, D. K.; Knüsel, P. N.; Bianchi, A.; Mauri, M.; Simonutti, R.; Norris, D. J.; et al. Photocatalytic Water-Splitting Enhancement by Sub-Bandgap Photon Harvesting. *ACS Appl. Mater. Interfaces* **2017**, *9*, 40180−40186.

(6) Ye, C.; Ma, J.; Han, P.; Chen, S.; Ding, P.; Sun, B.; Wang, X. Preparation and application of solid-state upconversion materials based on sodium polyacrylate. *RSC Adv.* **2019**, *9*, 17691−17697.

(7) Liu, Q.; Xu, M.; Yang, T.; Tian, B.; Zhang, X.; Li, F. Highly Photostable Near-IR-Excitation Upconversion Nanocapsules Based on Triplet−Triplet Annihilation for in Vivo Bioimaging Application. *ACS Appl. Mater. Interfaces* **2018**, *10*, 9883−9888.

(8) Park, J.; Xu, M.; Li, F.; Zhou, H.-C. 3D long-range triplet migration in a water-stable metal-organic framework for upconversion based ultralow-power in vivo imaging. *J. Am. Chem. Soc.* **2018**, *140*, 5493−5499.

(9) Pristash, S. R.; Corp, K. L.; Rabe, E. J.; Schlenker, C. W. Heavy-Atom-Free Red-to-Yellow Photon Upconversion in a Thiosquaraine Composite. *ACS Appl. Energy Mater.* **2019**, *3*, 19−28.

(10) Wei, Y.; Xian, H.; Lv, X.; Ni, F.; Cao, X.; Yang, C. Triplet−triplet annihilation upconversion with reversible emission-tunability induced by chemical-stimuli: a remote modulator for photocontrol isomerization. *Mater. Horiz.* **2021**, *8*, 606−611.

(11) Liu, M.; Wang, J.; Liang, G.; Luo, X.; Zhao, G.; He, S.; Wang, L.; Liang, W.; Li, J.; Wu, K. Spin-enabled photochemistry using nanocrystal-molecule hybrids. *Chem* **2022**, *8*, 1720−1733.

(12) Liang, W.; Nie, C.; Du, J.; Han, Y.; Zhao, G.; Yang, F.; Liang, G.; Wu, K. Near-infrared photon upconversion and solar synthesis using lead-free nanocrystals. *Nat. Photonics* **2023**, *17*, 346−353.

(13) Fujimoto, K.; Kawai, K.; Masuda, S.; Mori, T.; Aizawa, T.; Inuzuka, T.; Karatsu, T.; Sakamoto, M.; Yagai, S.; Sengoku, T.; et al. Triplet-Triplet Annihilation Based Upconversion Sensitized by a Reverse Micellar Assembly of Amphiphilic Ruthenium Complexes. *Langmuir* **2019**, *35*, 9740−9746.

(14) Tanaka, K.; Ohashi, W.; Inafuku, K.; Shiotsu, S.; Chujo, Y. Development of the sensitizer for generating higher-energy photons under diluted condition via the triplet-triplet annihilation-supported upconversion. *Dyes Pigm.* **2020**, *172*, 107821.

(15) Fan, C.; Wei, L.; Niu, T.; Rao, M.; Cheng, G.; Chruma, J. J.; Wu, W.; Yang, C. Efficient Triplet-Triplet Annihilation Upconversion with an Anti-Stokes Shift of 1.08 eV Achieved by Chemically Tuning Sensitizers. *J. Am. Chem. Soc.* **2019**, *141*, 15070−15077.

(16) Abulikemu, A.; Sakagami, Y.; Heck, C.; Kamada, K.; Sotome, H.; Miyasaka, H.; Kuzuhara, D.; Yamada, H. Solid-State, Near-Infrared to Visible Photon Upconversion via Triplet−Triplet Annihilation of a Binary System Fabricated by Solution Casting. *ACS Appl. Mater. Interfaces* **2019**, *11*, 20812−20819.

(17) Wei, Y.; Li, Y.; Li, Z.; Xu, X.; Cao, X.; Zhou, X.; Yang, C. Efficient Triplet-Triplet Annihilation Upconversion in Solution and Hydrogel Enabled by an S-T Absorption Os(II) Complex Dyad with an Elongated Triplet Lifetime. *Inorg. Chem.* **2021**, *60*, 19001−19008.

(18) Wei, Y.; Zheng, M.; Chen, L.; Zhou, X.; Liu, S. Near-infrared to violet triplet-triplet annihilation fluorescence upconversion of Os(ii) complexes by strong spin-forbidden transition. *Dalton Trans.* **2019**, *48*, 11763−11771.

(19) Wang, P.; Guo, S.; Wang, H. J.; Chen, K. K.; Zhang, N.; Zhang, Z. M.; Lu, T. B. A broadband and strong visible-light-absorbing photosensitizer boosts hydrogen evolution. *Nat. Commun.* **2019**, *10*, 3155.

(20) Shao, S.; Gobeze, H. B.; Bandi, V.; Funk, C.; Heine, B.; Duffy, M. J.; Nesterov, V.; Karr, P. A.; D'Souza, F. Triplet BODIPY and AzaBODIPY Derived Donor-acceptor Dyads: Competitive Electron Transfer versus Intersystem Crossing upon Photoexcitation. *ChemPhotoChem* **2020**, *4*, 68−81.

(21) Zhou, Q.; Zhou, M.; Wei, Y.; Zhou, X.; Liu, S.; Zhang, S.; Zhang, B. Solvent effects on the triplet−triplet annihilation upconversion of diiodo-Bodipy and perylene. *Phys. Chem. Chem. Phys.* **2017**, *19*, 1516−1525.

(22) Wu, W.; Guo, H.; Wu, W.; Ji, S.; Zhao, J. Organic triplet sensitizer library derived from a single chromophore (BODIPY) with long-lived triplet excited state for triplet-triplet annihilation based upconversion. *J. Org. Chem.* **2011**, *76*, 7056−7064.

(23) Quaglia, G.; Campana, F.; Latterini, L.; Vaccaro, L. Green Solvent Selection for Green-to-Blue Upconversion Based on TTA. *ACS Sustainable Chem. Eng.* **2022**, *10*, 9123−9130.

(24) Wei, Y.; Zhou, M.; Zhou, Q.; Zhou, X.; Liu, S.; Zhang, S.; Zhang, B. Triplet-triplet annihilation upconversion kinetics of C60-Bodipy dyads as organic triplet photosensitizers. *Phys. Chem. Chem. Phys.* **2017**, *19*, 22049−22060.

(25) Gonzalez Lopez, E. J.; Sarotti, A. M.; Martinez, S. R.; Macor, L. P.; Durantini, J. E.; Renfige, M.; Gervaldo, M. A.; Otero, L. A.; Durantini, A. M.; Durantini, E. N.; et al. BOPHY-Fullerene C60 Dyad as a Photosensitizer for Antimicrobial Photodynamic Therapy. *Chem.—Eur. J.* **2022**, *28*, No. e202103884.

(26) Heredia, D. A.; Durantini, A. M.; Durantini, J. E.; Durantini, E. N. Fullerene C60 derivatives as antimicrobial photodynamic agents. *J. Photochem. Photobiol., C* **2022**, *51*, 100471.

(27) Wu, W.; Zhao, J.; Sun, J.; Guo, S. Light-harvesting fullerene dyads as organic triplet photosensitizers for triplet-triplet annihilation upconversions. *J. Org. Chem.* **2012**, *77*, 5305.

(28) Fan, C.; Wu, W.; Chruma, J. J.; Zhao, J.; Yang, C. Enhanced Triplet−Triplet Energy Transfer and Upconversion Fluorescence through Host−Guest Complexation. *J. Am. Chem. Soc.* **2016**, *138*, 15405−15412.

(29) Liu, Y.; Lin, M.; Zhao, Y. Intersystem Crossing Rates of Isolated Fullerenes: Theoretical Calculations. *J. Phys. Chem. A* **2017**, *121*, 1145−1152.

(30) Öztürk, E.; Eserci, H.; Okutan, E. Perylenebisimide-fullerene dyads as heavy atom free triplet photosensitizers with unique singlet oxygen generation efficiencies. *J. Photochem. Photobiol., A* **2019**, *385*, 112022.

(31) Moor, K.; Kim, J.-H.; Snow, S.; Kim, J.-H. [C70] Fullerene-sensitized triplet−triplet annihilation upconversion. *Chem. Commun.* **2013**, *49*, 10829.

(32) Zhao, J.; Wu, W.; Sun, J.; Guo, S. Triplet photosensitizers: from molecular design to applications. *Chem. Soc. Rev.* **2013**, *42*, 5323−5351.

(33) Obondi, C. O.; Lim, G. N.; Karr, P. A.; Nesterov, V. N.; D'Souza, F. Photoinduced charge separation in wide-band capturing, multi-modular bis(donor styryl)BODIPY-fullerene systems. *Phys. Chem. Chem. Phys.* **2016**, *18*, 18187−18200.

(34) Bharmoria, P.; Bildirir, H.; Moth-Poulsen, K. Triplet-triplet annihilation based near infrared to visible molecular photon upconversion. *Chem. Soc. Rev.* **2020**, *49*, 6529−6554.

(35) Li, C.; Chen, G.; Zhang, Y.; Wu, F.; Wang, Q. Advanced Fluorescence Imaging Technology in the Near-Infrared-II Window for Biomedical Applications. *J. Am. Chem. Soc.* **2020**, *142*, 14789−14804.

(36) Sousa-Castillo, A.; Couceiro, J. R.; Tomas-Gamasa, M.; Marino-Lopez, A.; Lopez, F.; Baaziz, W.; Ersen, O.; Comesana-Hermo, M.; Mascarenas, J. L.; Correa-Duarte, M. A. Remote Activation of Hollow Nanoreactors for Heterogeneous Photocatalysis in Biorelevant Media. *Nano Lett.* **2020**, *20*, 7068−7076.

(37) Liu, K. K.; Song, S. Y.; Sui, L. Z.; Wu, S. X.; Jing, P. T.; Wang, R. Q.; Li, Q. Y.; Wu, G. R.; Zhang, Z. Z.; Yuan, K. J.; et al. Efficient Red/Near-Infrared-Emissive Carbon Nanodots with Multiphoton Excited Upconversion Fluorescence. *Adv. Sci.* **2019**, *6*, 1900766.

(38) Huang, L.; Wu, W.; Li, Y.; Huang, K.; Zeng, L.; Lin, W.; Han, G. Highly Effective Near-Infrared Activating Triplet-Triplet Annihilation Upconversion for Photoredox Catalysis. *J. Am. Chem. Soc.* **2020**, *142*, 18460−18470.

(39) Radiunas, E.; Raišys, S.; Juršėnas, S.; Jozeliūnaitė, A.; Javorskis, T.; Sinkevičiūtė, U.; Orentas, E.; Kazlauskas, K. Understanding the limitations of NIR-to-visible photon upconversion in phthalocyanine-sensitized rubrene systems. *J. Mater. Chem. C* **2020**, *8*, 5525−5534.

(40) Haruki, R.; Sasaki, Y.; Masutani, K.; Yanai, N.; Kimizuka, N. Leaping across the visible range: near-infrared-to-violet photon upconversion employing a silyl-substituted anthracene. *Chem. Commun.* **2020**, *56*, 7017−7020.

(41) Liang, H.; Liu, X.; Tang, L.; Mahmood, Z.; Chen, Z.; Chen, G.; Ji, S.; Huo, Y. Heavy atom-free triplet photosensitizer based on thermally activated delayed fluorescence material for NIR-to-blue triplet-triplet annihilation upconversion. *Chin. Chem. Lett.* **2023**, *34*, 107515.

(42) Wang, Z.; Huang, L.; Yan, Y.; El-Zohry, A. M.; Toffoletti, A.; Zhao, J.; Barbon, A.; Dick, B.; Mohammed, O. F.; Han, G. Elucidation of the Intersystem Crossing Mechanism in a Helical BODIPY for Low-Dose Photodynamic Therapy. *Angew. Chem., Int. Ed.* **2020**, *59*, 16114.

(43) Zhu, S. E.; Zhang, J. H.; Gong, Y.; Dou, L. F.; Mao, L. H.; Lu, H. D.; Wei, C. X.; Chen, H.; Wang, X. F.; Yang, W. Broadband Visible Light-Absorbing [70]Fullerene-BODIPY-Triphenylamine Triad: Synthesis and Application as Heavy Atom-Free Organic Triplet Photosensitizer for Photooxidation. *Molecules* **2021**, *26*, 1243.

(44) Tomasi, J.; Mennucci, B.; Cammi, R. Quantum Mechanical Continuum Solvation Models. *Chem. Rev.* **2005**, *105*, 2999−3094.

(45) Frisch, M. J.; Trucks, G. W.; Schlegel, H. B.; Scuseria, G. E.; Robb, M. A.; Cheeseman, J. R.; Scalmani, G.; Barone, V.; Petersson, G. A.; Nakatsuji, H.; et al. *Gaussian 16*, Revision B.01: Wallingford, CT, 2016.

(46) Vandewal, K.; Benduhn, J.; Nikolis, V. C. How to determine optical gaps and voltage losses in organic photovoltaic materials. *Sustainable Energy Fuels* **2018**, *2*, 538−544.

(47) Liu, J.-Y.; Hou, X.-N.; Tian, Y.; Jiang, L.; Deng, S.; Röder, B.; Ermilov, E. A. Photoinduced energy and charge transfer in a bis(triphenylamine)−BODIPY−C60 artificial photosynthetic system. *RSC Adv.* **2016**, *6*, 57293−57305.

(48) Wei, Y.; Zheng, M.; Zhou, Q.; Zhou, X.; Liu, S. Application of a bodipy−C70 dyad in triplet−triplet annihilation upconversion of perylene as a metal-free photosensitizer. *Org. Biomol. Chem.* **2018**, *16*, 5598−5608.

(49) Wang, Z.; Zhao, J.; Di Donato, M.; Mazzone, G. Increasing the anti-Stokes shift in TTA upconversion with photosensitizers showing red-shifted spin-allowed charge transfer absorption but a non-compromised triplet state energy level. *Chem. Commun.* **2019**, *55*, 1510−1513.

(50) Dong, Y.; Sukhanov, A. A.; Zhao, J.; Elmali, A.; Li, X.; Dick, B.; Karatay, A.; Voronkova, V. K. Spin−Orbit Charge-Transfer Intersystem Crossing (SOCT-ISC) in Bodipy-Phenoxazine Dyads: Effect of Chromophore Orientation and Conformation Restriction on the Photophysical Properties. *J. Phys. Chem. C* **2019**, *123*, 22793−22811.

(51) Wang, Z.; Zhao, J. Bodipy-Anthracene Dyads as Triplet Photosensitizers: Effect of Chromophore Orientation on Triplet-State Formation Efficiency and Application in Triplet-Triplet Annihilation Upconversion. *Org. Lett.* **2017**, *19*, 4492−4495.

(52) Chen, H.; An, N.; Wang, Y.; Wang, G.; Mukherjee, S.; Bian, H.; Ma, J.; Liu, J.; Fang, Y. Tracking the Intramolecular Charge Transfer

Process of 2,6-Substituted D-A BODIPY Derivatives. *J. Phys. Chem. B* **2023**, *127*, 2044−2051.

(53) Wei, Y.; Wang, Y.; Zhou, Q.; Zhang, S.; Zhang, B.; Zhou, X.; Liu, S. Solvent effects on triplet−triplet annihilation upconversion kinetics of perylene with a Bodipy-phenyl-C60 photosensitizer. *Phys. Chem. Chem. Phys.* **2020**, *22*, 26372−26382.

(54) Shokri, S.; Wiederrecht, G. P.; Gosztola, D. J.; Ayitou, A. J.-L. Photon Upconversion Using Baird-Type (Anti)Aromatic Quinoidal Naphthalene Derivative as a Sensitizer. *J. Phys. Chem. C* **2017**, *121*, 23377−23382.

(55) Xiao, X.; Tian, W.; Imran, M.; Cao, H.; Zhao, J. Controlling the triplet states and their application in external stimuli-responsive triplet-triplet-annihilation photon upconversion: from the perspective of excited state photochemistry. *Chem. Soc. Rev.* **2021**, *50*, 9686−9714.

(56) Orlandi, G.; Negri, F. Electronic states and transitions in C60 and C70 fullerenes. *Photochem. Photobiol. Sci.* **2002**, *1*, 289−308.

(57) Olesund, A.; Johnsson, J.; Edhborg, F.; Ghasemi, S.; Moth-Poulsen, K.; Albinsson, B. Approaching the Spin-Statistical Limit in Visible-to-Ultraviolet Photon Upconversion. *J. Am. Chem. Soc.* **2022**, *144*, 3706−3716.

(58) Turshatov, A.; Busko, D.; Kiseleva, N.; Grage, S. L.; Howard, I. A.; Richards, B. S. Room-Temperature High-Efficiency Solid-State Triplet−Triplet Annihilation Up-Conversion in Amorphous Poly-(olefin sulfone)s. *ACS Appl. Mater. Interfaces* **2017**, *9*, 8280−8286.

(59) Olmsted, J. Calorimetric determinations of absolute fluorescence quantum yields. *J. Phys. Chem.* **1979**, *83*, 2581−2584.

(60) Zhou, Y.; Castellano, F. N.; Schmidt, T. W.; Hanson, K. On the Quantum Yield of Photon Upconversion via Triplet−Triplet Annihilation. *ACS Energy Lett.* **2020**, *5*, 2322−2326.

(61) Monguzzi, A.; Mezyk, J.; Scotognella, F.; Tubino, R.; Meinardi, F. Upconversion-induced fluorescence in multicomponent systems: Steady-state excitation power threshold. *Phys. Rev. B: Condens. Matter Mater. Phys.* **2008**, *78*, 195112.

(62) Cheng, Y. Y.; Fückel, B.; Khoury, T.; Clady, R. G.; Tayebjee, M. J.; Ekins-Daukes, N.; Crossley, M. J.; Schmidt, T. W. Kinetic Analysis of Photochemical Upconversion by Triplet− Triplet Annihilation: Beyond Any Spin Statistical Limit. *J. Phys. Chem. Lett.* **2010**, *1*, 1795−1799.

(63) Haefele, A.; Blumhoff, J.; Khnayzer, R. S.; Castellano, F. N. Getting to the (Square) Root of the Problem: How to Make Noncoherent Pumped Upconversion Linear. *J. Phys. Chem. Lett.* **2012**, *3*, 299−303.

(64) Schmidt, T. W.; Castellano, F. N. Photochemical upconversion: the primacy of kinetics. *J. Phys. Chem. Lett.* **2014**, *5*, 4062−4072.

(65) Merrifield, R. E. Magnetic effects on triplet exciton interactions. *Pure Appl. Chem.* **1971**, *27*, 481−498.

(66) Yago, T.; Tashiro, M.; Hasegawa, K.; Gohdo, M.; Tsuchiya, S.; Ikoma, T.; Wakasa, M. Triplet-Triplet Annihilation via the Triplet Channel in Crystalline 9,10-Diphenylanthracene. *J. Phys. Chem. Lett.* **2022**, *13*, 8768−8774.

(67) Hoseinkhani, S.; Tubino, R.; Meinardi, F.; Monguzzi, A. Achieving the photon up-conversion thermodynamic yield upper limit by sensitized triplet-triplet annihilation. *Phys. Chem. Chem. Phys.* **2015**, *17*, 4020−4024.

(68) Sun, W.; Ronchi, A.; Zhao, T.; Han, J.; Monguzzi, A.; Duan, P. Highly efficient photon upconversion based on triplet−triplet annihilation from bichromophoric annihilators. *J. Mater. Chem. C* **2021**, *9*, 14201−14208.